STELLAR POPULATION STUDIES WITH THE SDSS. I. THE VERTICAL DISTRIBUTION OF STARS IN THE MILKY WAY[1]

Bing Chen,[2] Chris Stoughton,[3] J. Allyn Smith,[4] Alan Uomoto,[2] Jeffrey R. Pier,[5] Brian Yanny,[3] Željko Ivezić,[6] Donald G. York,[7] John E. Anderson,[3] James Annis,[3] Jon Brinkmann,[8] István Csabai,[2,9] Masataka Fukugita,[10] Robert Hindsley,[11] Robert Lupton,[6] and Jeffrey A. Munn[5]
(for the SDSS Collaboration)

ABSTRACT

We present star count data from the Sloan Digital Sky Survey for 5.8×10^5 stars brighter than $g' = 21$ mag over 279 deg^2 in two samples north and south of the Galactic plane. Using these high-latitude ($49° < |b| < 64°$) star counts we determine the Sun's distance from the Galactic midplane to be 27 ± 4 pc and the scale height of the old thin disk to be 330 ± 3 pc. Because of the photometric accuracy and large area sky coverage of these data, the color-magnitude diagram clearly reveals a significant thick-disk population distinct in color from a Galactic halo population. The position of the thick-disk turnoff is at $g' - r' \sim 0.33$. Several questions about the existence of the thick disk and its origin are addressed through a set of model fits to the star count data. Our best-fit model gives a thick-disk scale height between 580 and 750 pc, below the original proposal of Gilmore and Reid, and the corresponding space number density normalization is 13%–6.5% of the thin disk. The conclusions reached in this paper favor a scenario in which the thick disk formed through the heating of a preexisting thin disk, with the heating mechanism being the merging of a satellite galaxy.

The density law for the Galactic halo population is also investigated. We find that the data support a flattened halo with $c/a \sim 0.55 \pm 0.06$ and a relatively flat power-law index (2.5 ± 0.3). The axis ratio of the visible halo found in this paper is compatible with that of dark halo, suggesting that they have the same shape and dynamical origin.

Subject headings: Galaxy: stellar content — Galaxy: structure

1. INTRODUCTION

Over the last two decades highly efficient, linear, two-dimensional detectors, along with powerful data processing systems, have enabled the generation of large quantities of high-quality imaging data. New and more accurate star count surveys have been published (Majewski 1991; Ojha et al. 1996; Spagna et al. 1996; Phleps et al. 2000) or are being carried out (York et al. 2000). The main structural features of the Milky Way have been identified. As a consequence, it has been possible to design synthetic models of Galactic stellar populations (Bahcall & Soneira 1981; Gilmore 1984; Robin & Crézé 1986; Reid & Majewski 1993; Méndez & van Altena 1998; Chen et al. 1999).

Our knowledge of details of the structure of the Milky Way, as inferred from star count data with color information, is about to enter the next level of precision with the advent of new surveys such as the Sloan Digital Sky Survey (SDSS). This will, in turn, require the refinement of models of Galactic structure to fit parameters of the basic components of our Galactic star system.

Bahcall & Soneira (1981) established the first self-consistent model by analyzing star count data from Kron (1978), Tyson & Jarvis (1979), and Peterson et al. (1979). In their model, old thin disk stars were found to have a scale height of 325 pc, and the halo stars were represented by a deprojected de Vaucouleurs $r^{1/4}$ law. Bahcall & Soneira (1984) and Bahcall et al. (1985) showed that all the existing star count data with $V < 22$ mag could be successfully modeled with only two populations, thin-disk and spheroid.

By analyzing data near the south Galactic pole from the UK Schmidt Telescope, Gilmore (1984) proposed a Galaxy model with three populations: thin-disk, thick-disk, and halo. The scale height of the thick disk was found to be 1450 pc and its space number density 2% of the thin disk in the solar neighborhood.

Robin et al. (1996) analyzed star count data in a number of Galactic directions. They found that the scale height of the thick disk is 760 pc and that its density is 6% of the thin disk. In Table 1, we summarize the main parameters relating to the vertical distribution of stars in these models.

To pin down Galactic structure with more precision, a data set with high photometric accuracy is required. Furthermore, the observed area should be large enough to minimize the effects of local fluctuations in the spatial distribution of stars. The Sloan Digital Sky Survey (York et al. 2000) is producing high-quality ($\sim 3\%$ photometry at

TABLE 1

MODELS FOR THE GALAXY

Parameter	Bahcall & Soneira (1984)	Gilmore (1984)	Robin et al. (2000)	This Paper
Thin Disk:				
Density law	Exponential	Exponential	Einasto (1979)	Exponential
Scale height (pc)	90–325	90–325	90–270	90–325
Thick Disk:				
Density law	...	Exponential	Exponential	Exponential
Scale height (pc)	...	1300	750	580–750
Local normalization......	...	2%	5.6%	13%–6.5%
Halo:				
Density law	de Vaucouleurs	de Vaucouleurs	Power law	Power law
Local normalization......	0.150%	0.125%	1.64×10^{-4} stars pc^{-3}	0.125%
Minor/major axis.........	0.80	0.80	0.76	0.55
Power-law index	...	...	2.44	2.5

$g' \sim 19$) imaging data over large areas of the sky (10,000 deg^2 by survey completion). The morphological and color information allow robust star-galaxy-quasar separation. These data, which contain valuable information about the Galaxy and its stellar components, allow us to separate the different stellar populations and therefore confidently constrain Galactic structure parameters.

In this paper, we use SDSS star counts to investigate the vertical distribution of stars in the Milky Way. In Section 2, we summarize the SDSS data used in the paper. Section 3 discusses the main structural parameters of our Galaxy model. We emphasize that the main conclusions in this paper do not depend on the specific choice of a model. In § 4, we use samples from above and below the Galactic plane to determine the scale height of the thin disk and the Sun's distance from the Galactic midplane. Section 5 shows the g^*, g^*-r^* color-magnitude diagram (CMD) for $\sim 5.8 \times 10^5$ stars, in which one can clearly visualize the thick-disk population. In § 6, we investigate the vertical distribution of the Galactic thick disk, and the density law for the halo population of the Galaxy is discussed in § 7. The conclusions are summarized in § 8.

2. OBSERVATIONS

SDSS is designed to acquire uniform and accurate five-color catalogs of objects. The SDSS imaging camera (Gunn et al. 1998) consists of a mosaic of 30 2048×2048 CCDs for primary imaging and an additional 24 400×2048 CCDs for astrometric and focus measurements. The sky is imaged in drift-scan mode through five broadband filters, u', g', r', i', and z', with effective wavelengths of 3540 Å, 4760 Å, 6280 Å, 7690 Å, and 9250 Å, complete to limiting (5:1 signal-to-noise) point-source magnitudes of 22.3, 23.3, 23.1, 22.3, and 20.8, respectively. The imaging CCDs are arranged in six columns of five CCDs each. The five CCDs in each column view the sky through the five different bandpasses in succession. Pixels subtend 0″.4 on the sky. The exposure time in each band is 54.1 s. A "run" generates six 13′.5 wide parallel continuous strips of sky ("scan lines") along a great circle, with a gap of 11′.5 between columns. A second run, offset 12′.5 from the first, is obtained to interlace the two runs (with a 1′ overlap on each scan line edge) into a fully imaged 2°.5 wide "stripe" on the sky.

The calibration and definition of the $u'g'r'i'z'$ standard-star system was accomplished using the 1 m Ritchey-Chrétien telescope at the US Naval Observatory Flagstaff Station (Smith et al. 2001). An auxiliary 0.5 m telescope at Apache Point Observatory (site of the SDSS 2.5 m survey telescope) repeatedly measures $u'g'r'i'z'$ standard stars to determine extinction and uses those measures to calibrate fainter stars in a set of secondary patches of sky. The secondary patches are located across every 15° of survey longitude along every survey stripe. Magnitudes in this paper are quoted in the $u^*g^*r^*i^*z^*$ system to differentiate them from the final, calibrated SDSS photometric system ($u'g'r'i'z'$), which was uncertain at the ~ 0.05 mag level at the time of the observations and reductions discussed in this paper.

The photometric pipeline (Lupton et al. 2001) reduces the imaging data and measures relative positions, magnitudes, colors, and shape parameters for all detected objects in the images. The relative positions are transformed to absolute positions using transformations derived from the astrometric pipeline (Pier et al. 2001). The data processing system (Adelman et al. 1999) consists of two Compaq Digital Alpha systems, 2 Tbytes of disk storage, and an SGI Origin 2000 system running the database. Calibrated data are sent to collaborating institutions automatically.

For this analysis we use two stripes of data in the equatorial region $|\delta| < 1°.3$. The northern sample (north of the Galactic plane, hereafter NGS) is a filled stripe from SDSS runs 752 and 756, obtained 1999 March 21 and 22. The southern sample (south of the Galactic plane, hereafter SGS) is a filled stripe from SDSS runs 94 and 125, obtained 1998 September 19 and 25. Most of these regions have been scanned twice. The additional observations are used to verify the findings in the primary runs. A detailed description of the samples can be found in Yanny et al. (2000). In order to avoid low Galactic latitude regions, where correcting for interstellar reddening is problematic, in this paper NGS includes only objects with $165° <$ R.A. $< 225°$ and SGS those with $-6° <$ R.A. $< 45°$. Figure 1 shows the regions of the SGS and NGS in Galactic coordinates, which cover 128 and 151 deg^2 on the sky, respectively. Both SGS and NGS are limited to $49° < |b| < 64°$. While the two samples are drawn from the same range in $|b|$, differences in Galactic longitude account for the difference in mean stellar density between the two samples.

Sample contamination from quasars in our samples is negligible. Most quasars are separable in the SDSS photometric system because of their unusual positions in color-color diagrams (Fan 1999). The low-redshift quasars can be distinguished from stars by their bluer u^*-g^* color (Ivezić
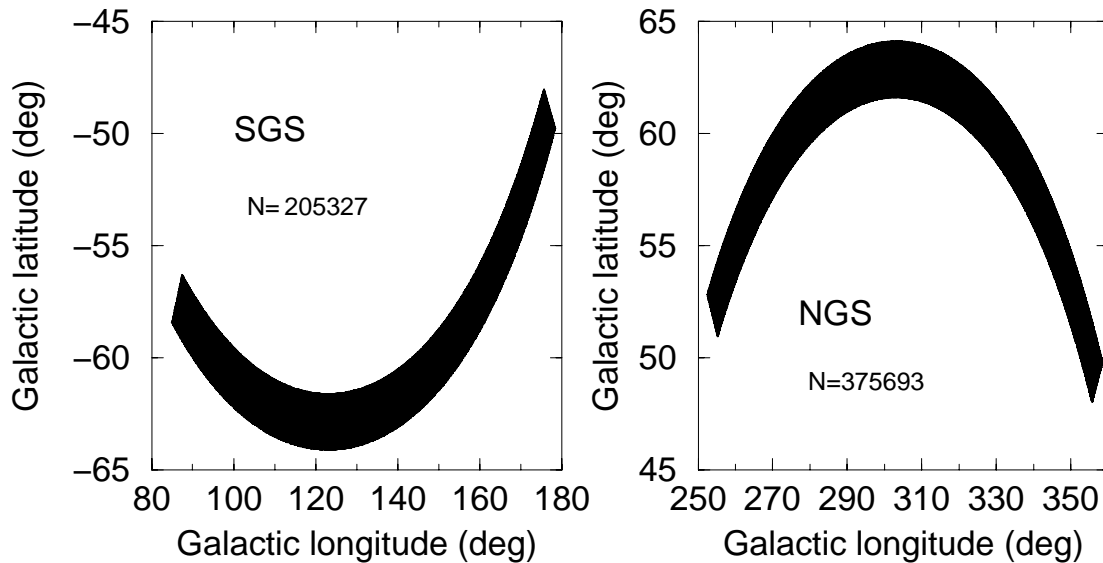
Fig. 1.—SGS and NGS sample regions in Galactic coordinates. SGS and NGS include 205,327 and 375,693 stellar objects and cover 128 and 151 deg² in the sky, respectively.

et al. 2000). In this study, we limit our sample with $u^{*} - g^{*} > 0.5$ in order to remove these extragalactic objects. Finally, our SGS and NGS include 205,327 and 375,693 objects with $15 < g^{*} < 21$, respectively.

3. GALAXY MODEL

A Galaxy model has been developed for interpreting star counts in the north Galactic pole (Chen 1997) and four regions at low Galactic latitudes (Chen et al. 1999). The model simulates the expected star counts by integrating a luminosity function weighted by the space density of stars with respect to the volume element over an observed area. The luminosity function is mainly derived from nearby stars. The density distribution of stars is adopted from photometric profiles of various external galaxies and is expressed by an analytic function leaving a few numerical parameters to be determined. The main structure parameters in our model are summarized in Table 2. In the following paragraphs we give a short description of the parameters adopted from previous investigations. Other parameters concerning the vertical distribution of stars will be investigated in subsequent sections. For disk stars, the adopted luminosity function is that derived by Wielen, Jahreiss, & Kruger (1983) from observations of nearby stars. The stellar density law used for the disk is a double exponential (Gilmore 1984; Bahcall 1986; Reid & Majewski 1993). The (M_V, $B-V$) CMD (Bahcall & Soneira 1984) is constructed from main-sequence data given by Johnson (1965, 1966) and Keenan (1963), with the giant branch assumed to be the same as given by Morgan & Eggleton (1978) for M67. Most disk-density scale length determinations range between 1.8 and 6 kpc (Méndez & van Altena 1998). We adopted a scale length of 2250 pc (Chen et al. 1999).

The halo luminosity function is assumed to be similar in shape to that of the disk (Bahcall & Soneira 1984). This luminosity function resembles the measured luminosity functions of globular clusters in the Galaxy and is consistent with the Schmidt (1975) data on high-velocity stars. We use the CMD of M13 (Sandage 1970), with [Fe/H] ~ -1.4,

because it provides a good fit to much of the high-latitude data (Bahcall & Soneira 1984). We adopt a halo-to-disk stellar density ratio in the solar neighborhood of 0.00125.

The thick-disk luminosity function is assumed to be similar in shape to that of the disk (Robin & Crézé 1986). The stellar density law used for the thick disk is a double exponential function (Gilmore 1984; Reid & Majewski 1993). The adopted CMD is that of 47 Tuc, with [Fe/H] $= -0.7$ (Reid & Majewski 1993).

We have allowed for an offset in the distance of the Sun from the Galactic plane in our model. A three-dimensional extinction distribution (Chen et al. 1999) has been adopted in our Galaxy model code. However, the average reddening (E_{B-V}) in both samples is about 0.02–0.03 mag, so it is not significant in our studies.

TABLE 2

MAIN STRUCTURE PARAMETERS IN OUR GALAXY MODEL

| Parameter	Value/Reference
Solar distance from the plane (pc)	27 (derived)
Disk population:	
Luminosity function	Wielen et al. (1983)
Color-magnitude diagram	Bahcall & Soneira (1984)
Density law	Double exponential
Scale length (pc)	2250
Scale height, late-type dwarfs (pc)...	330 (derived)
Thick-disk population:	
Luminosity function	Wielen et al. (1983)
Color-magnitude diagram	47 Tuc
Density law	Double exponential
Scale length (pc)	3500
Scale height (pc)	580–750 (derived)
Local normalization (%)	13%–6.5% (derived)
Halo population:	
Luminosity function	M13
Color-magnitude diagram	M13
Density law	Power law
Axial ratio	0.55 (derived)
Local normalization (%)	0.125
Extinction model [$A_v(r, l, b)$]	NCI model (Chen et al. 1999)
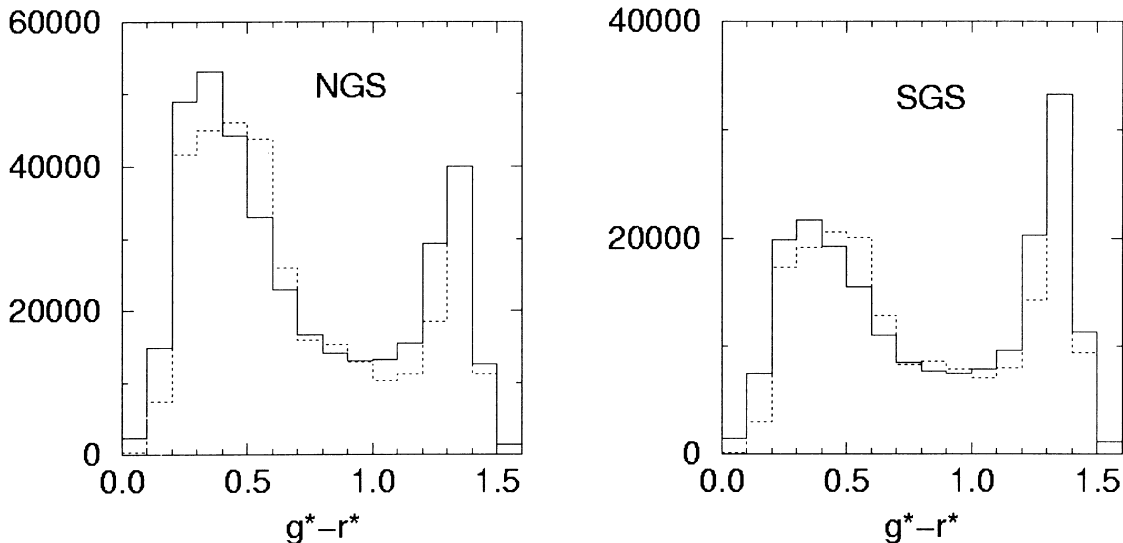
FIG. 2.—The g^*-r^* color distribution of model simulations (*dashed lines*) and observations (*solid lines*) in SGS and NGS

In this paper, a version of the SDSS standard photometric system (Smith et al. 2001) is used to calculate color transformations as follows:

$$g^* = V + 0.53(B-V) - 0.075 , \qquad (1)$$

$$r^* = V - 0.438(B-V) + 0.12 , \qquad (2)$$

and

$$u^* - g^* = 1.32(U-B) + 0.13 . \qquad (3)$$

These transformations are valid for stellar-type spectral-flux distributions over a wide range of colors ($-0.5 < g'-r' < 2.2$). A comparison between Fukugita et al. (1996) and these transformations shows that the differences between the theoretical transforms of Fukugita et al. (1996) and the empirical transforms of Smith et al. (2001) are less than 0.02 mag. The formal accuracy of this transformation relation is about 0.04 mag. In Figure 2 we compare the g^*-r^* color distribution between the model simulations and observations in SGS and NGS. The model is the best-fitting model described in detail below. The observed counts in SGS and NGS are shown by solid lines, and the dashed lines represent model simulations.

Figure 3 shows the differential number counts in NGS and SGS. In this figure we can see that observations do not include enough stars at $g^* < 15$, because stars this bright are saturated in the SDSS imaging camera. However, we can see that both samples are complete to at least $g^* \sim 21$ (see Figs. 2 and 5 of Yanny et al. 2000).

In general, the model counts agree well with the observations over a range of observed magnitude and color in both regions. We find that our model represents well the observed stellar content of the Galaxy. This model provides an interpretation of the observations, and such an interpretation is what is initially needed to direct our studies to ever better models and better understanding.

4. THIN-DISK SCALE HEIGHT AND SUN'S DISTANCE FROM THE GALACTIC PLANE

The displacement of the Sun from the center of the Galactic plane has an important effect on the interpretation of the density distribution of objects when we look out of the

plane (Méndez & van Altena 1998). Contemporary estimates differ, but all lie in the range 5–40 pc north of the Galactic plane. Stothers & Frogel (1974) determined $Z_{sun} = 24 \pm 3$ pc from B0–B5 stars within 200 pc of the Sun, Pandey, Bhatt, & Mahra (1988) obtained 28 ± 5 pc from an examination of the distribution of open clusters, and Conti & Vacca (1990) found 15 ± 3 pc from a sample of 101 Wolf-Rayet stars. Humphreys & Larsen (1995) have determined $Z_{sun} = 20.5 \pm 3.5$ pc from star counts in 12 Palomar Sky Survey fields. Méndez & van Altena (1998) and Chen et al. (1999) derived 27 ± 3 pc from a comparison between model simulations and star counts in several low-latitude fields. Stobie & Ishida (1987) and Yamagata & Yoshii (1992) found that the Sun is situated at 40 ± 3 pc, based on high-latitude star counts. Infrared counts have offered a valuable complementary perspective on the value of Z_{sun}. Hammersley et al. (1995) found 15.5 pc from *COBE, IRAS,* and Two-Micron Galactic Survey data, Cohen (1995) obtained 15 pc based on *IRAS* source counts, and Binney, Gerhard, & Spergel (1997) derived a value of $Z_{sun} = 14$ pc above the plane from a dust-corrected near-infrared *COBE* DIRBE surface brightness map of the inner Galaxy.

Red dwarfs reside on the reddest part of g^*-r^* color distributions. We use these stars (with $15 < g^* < 18$ and $g^*-r^* > 1.2$) to investigate the sun's distance from the center of the Galactic plane and the thickness of the old (thin) disk. From the observed samples, there are 6425 of these stars in SGS and 6775 in NGS.

Often, the density of the disk is assumed to have the following form:

$$n(r,z) \sim \exp\left(-\frac{R-R_o}{h_l}\right) \exp\left(-\frac{|z|}{h_z}\right) \qquad (4)$$

(see, e.g., Bahcall & Soneira 1981), where $z = Z_o + r(\sin b)$, r is the distance to the object from the sun, R is the Galactocentric distance in the plane, and h_z and h_l are the scale height and scale length of old disk, respectively. To determine Z_o from the observed counts, we generated a set of simulated star catalogs with various disk scale heights and solar displacements from the Galactic plane.

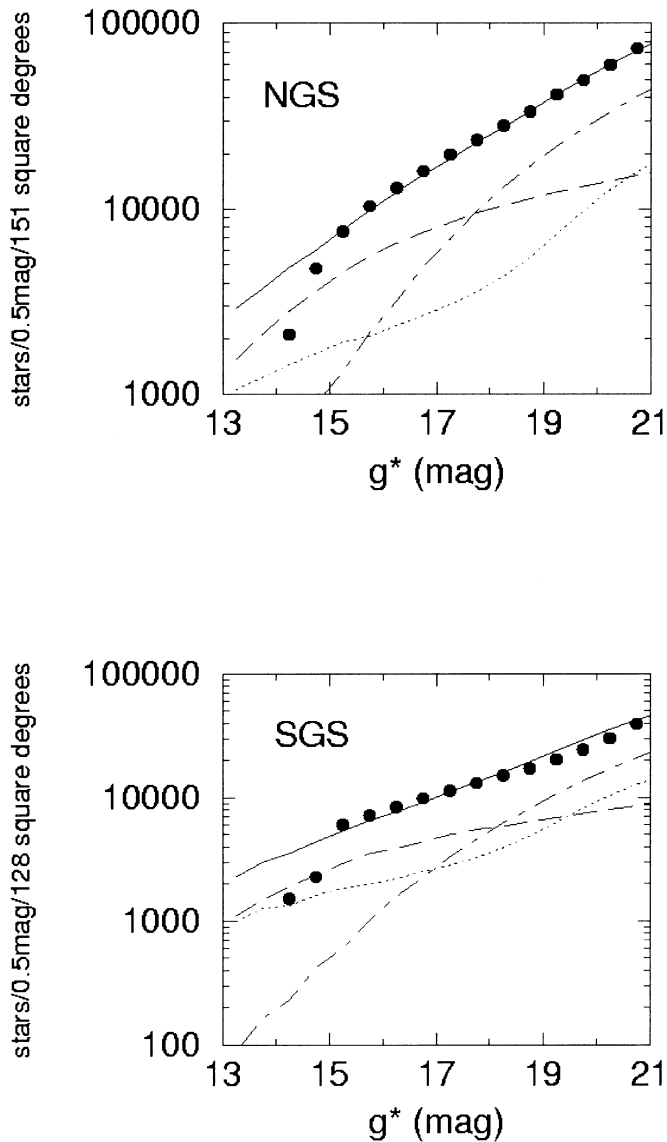For each model, we simulate catalogs of data similar to the observed data sets, then we compare the simulations

FIG. 3.—Differential number count $A(g^*)$ of stars at interval of 0.5 mag plotted against g'. The observed counts are shown as circles. The dotted, dashed, and dot-dashed lines represent predicted contributions of the thin disk, thick disk, and halo, respectively, and the solid line represents their sum.

with the observations in the SGS and NGS simultaneously and derive a best-fit model for the Sun's displacement and the old-disk scale height.

The result is shown in Figure 4, where the x-axis gives the number of stars predicted for the SGS and the y-axis the number of stars predicted for the NGS. The solid circle is the observation. Model predictions are shown along four dotted lines, each corresponding to a particular old thin disk scale height ($h_z = 275$, 300, 325, and 350 pc). For each dotted line, five open circles mark particular Z_o-values (from $Z_o = 0$ on the left to $Z_o = 40$ pc on the right). Comparing the observed value with the model predictions, we find the best fit gives a scale height of 330 pc for old-disk stars and a Z_o of 27 pc for the Sun's distance from the Galactic plane.

To estimate the observed errors for these findings, we divide SGS and NGS into 10 subsamples each. Table 3 shows the derived Z_o and h_z for each subsample. From the subsample results, we find the observed errors to be $\sigma_{Z_o} = 3$ pc and $\sigma_{h_z} = 4$ pc.

In our analysis, we assumed a thin-disk scale length h_l of 2250 pc. In order to consider the effect of errors in the thin-disk scale length in our determination, we performed the same analysis using a large scale length, 3250 pc, the value adopted by Bahcall & Soneira (1981) and Gilmore (1984) in their models. The open circles in Figure 5 show the result, indicating that thin-disk scale length is not important in our determination of the Sun's distance from the Galactic midplane and the thin-disk scale height.

A thick-disk scale height of 580 pc and a local density of 13% of the thin disk have been adopted in Figure 4 (and will be justified in § 5). In order to investigate the influence of the choice of the thick-disk population on the scale height of the thin disk, we carried out the same thin-disk analysis with a thick-disk scale height of 750 pc and local density of 6.5% of the thin disk. The results are plotted as asterisks in Figure 5. We found that these alternative thick-disk parameters do not change our determination of thin-disk scale height significantly.

Most stars in this section have absolute magnitudes M_V between 8 and 12 mag. In such a range of absolute magnitude, the Wielen et al. (1983) luminosity function is in good agreement with other determinations (McCuskey 1966;

TABLE 3

MEASUREMENTS DERIVED FROM 10 SUBSAMPLES IN NGS AND SGS

Subsample	NGS	SGS	N_{SGS}	N_{NGS}	Z_o (pc)	h_z (pc)
1...........	$-6 <$ R.A. ≤ -0.9	$165 <$ R.A. < 171	657	665	20	320
2...........	$-0.9 <$ R.A. ≤ 4.2	$171 <$ R.A. < 177	613	716	0	330
3...........	$4.2 <$ R.A. ≤ 9.3	$177 <$ R.A. < 183	631	611	30	320
4...........	$9.3 <$ R.A. ≤ 14.4	$183 <$ R.A. < 189	623	594	30	310
5...........	$14.4 <$ R.A. ≤ 19.5	$189 <$ R.A. < 195	647	675	35	345
6...........	$19.5 <$ R.A. ≤ 24.6	$195 <$ R.A. < 201	622	641	35	320
7...........	$24.6 <$ R.A. ≤ 29.7	$201 <$ R.A. < 207	629	669	30	320
8...........	$29.7 <$ R.A. ≤ 34.8	$207 <$ R.A. < 213	665	710	35	335
9...........	$34.8 <$ R.A. ≤ 39.9	$213 <$ R.A. < 219	647	728	30	330
10	$39.9 <$ R.A. ≤ 45.0	$219 <$ R.A. < 225	691	766	45	345

NOTES.—N_{SGS} and N_{NGS} are the numbers of stars in the given range of R.A. in SGS and NGS, respectively. Z_o is the Sun's distance from the Galactic plane, and h_z is the scale height for the old thin disk.
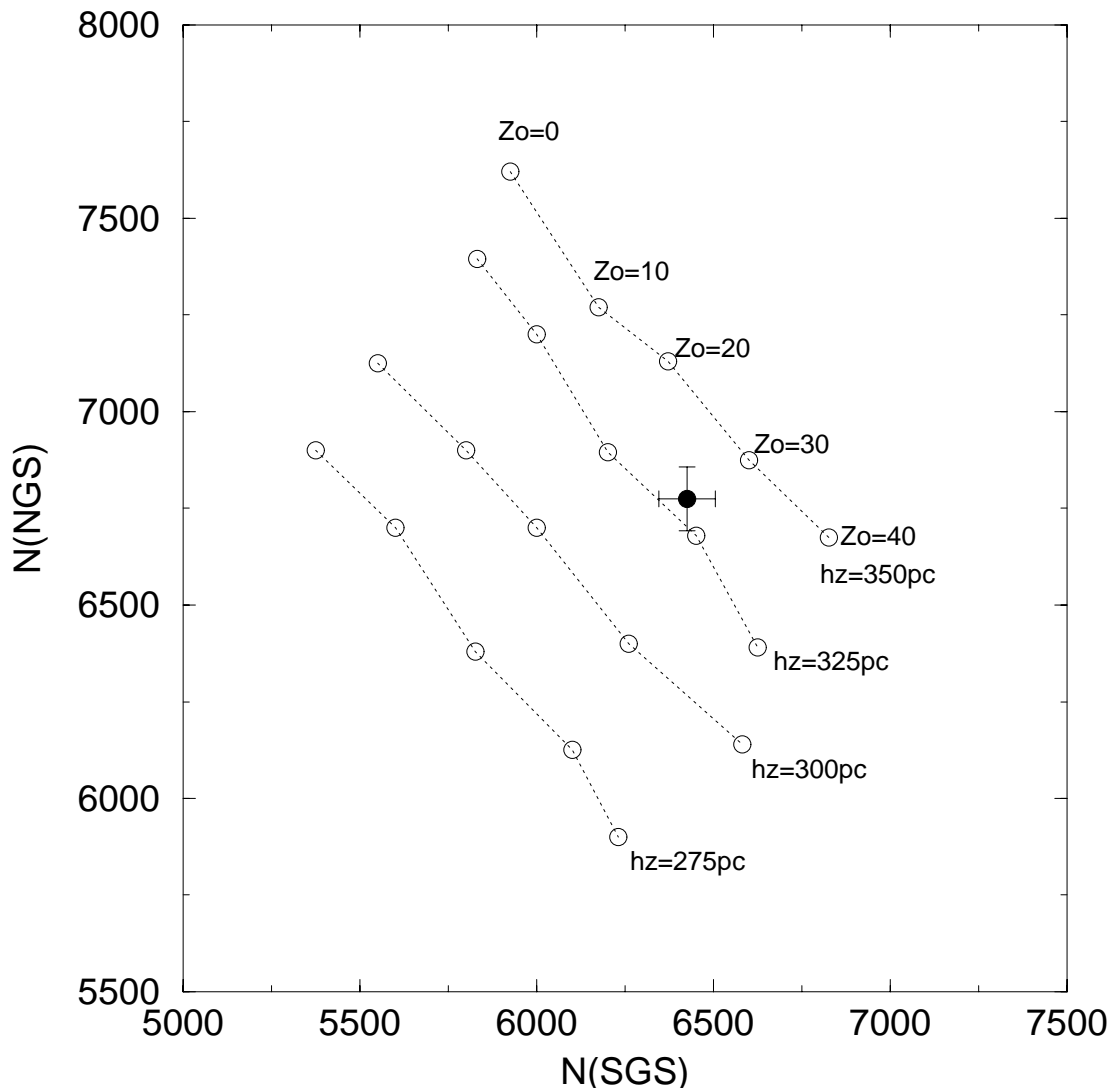
FIG. 4.—Number of SGS stars on x-axis and NGS stars on y-axis. The solid circle shows observed result. Model predictions are shown in four dotted lines. Each dotted line corresponds to a given old thin disk scale height, and for each dotted line, five open circles are the values predicted by the model for a given Z_o (from $Z_o = 0$ at left to $Z_o = 40$ pc at right).

Robin & Crézé 1986). So the influence of the choice of the disk luminosity function on our results is negligible.

One complication in the interpretation of the differences between southern and northern star counts could arise from an asymmetric distribution of absorbing matter. This would require a differential interstellar extinction A_v greater by 0.5 mag in the northern sky than in the southern sky. However, there is no evidence for such a color difference in the $g^* - r^*$ distribution of the southern and northern data. Furthermore, such a high reddening is not in agreement with other observational data.

Several results for the old thin disk scale height have been published in the literature. Most authors (Gilmore 1984; Bahcall & Soneira 1984; Yoshii, Ishida, & Stobie 1987; Reid & Majewski 1993) find a scale height of ∼325 pc for old-disk stars, but Kuijken & Gilmore (1989) derived a scale height of 249 pc for the old-disk stars, Haywood, Robin, & Crézé (1997) showed that the overall vertical density of the Galactic disk is close to an exponential with scale height about 250 pc, and Ojha et al. (1999) showed that the scale height of the thin disk is 240 pc based on an analysis of two

star count samples. Our results (330 pc) are consistent with the classical value in the literature.

5. THE THICK DISK AS A DISTINCT POPULATION IN THE GALAXY

The existence of a thick-disk component in our Galaxy, in addition to the thin disk and the halo, has been a matter of controversy. Gilmore & Reid (1983) derived the vertical density profile for the Galaxy and were the first to identify a thick-disk population by star count data toward the south Galactic pole. Some studies (Gilmore & Reid 1983; Ratnatunga & Yoss 1991; Robin et al. 1996; Ojha et al. 1999; Buser, Rong, & Karaali 1999) showed evidence that a thick-disk component is necessary to fit observed samples, although the structural parameters for this population are not well determined. However, it has also been argued that only two main components are needed to explain the observational data and that the thick disk simply represents an overlap of the two main distributions. Bahcall (1986) used distributions in colors and magnitudes of stars to set constraints on Galactic model parameters. He showed that two
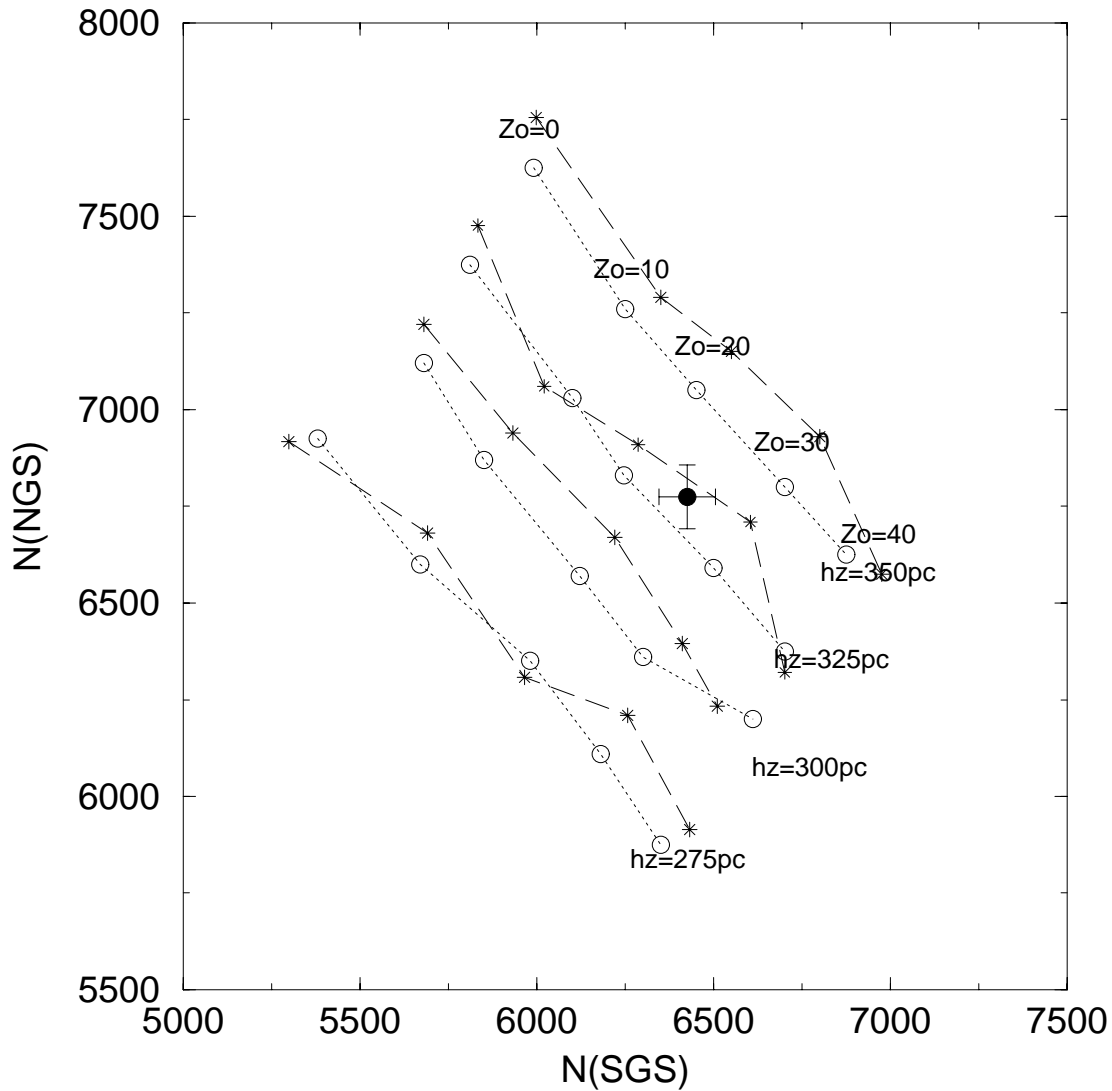
Fig. 5.—Same as Fig. 4, but open circles are plotted using a thin-disk scale length h_l of 3250 pc. Asterisks are plotted using a thick-disk scale height of 750 pc and local density of 6.5% of the thin disk.

components were sufficient to model the star count data with the data's (then) typical color errors of $\sim 20\%$. Majewski (1991) pointed out that either the three-component or the two-component structure might be consistent with his deep star count sample at the north Galactic pole. Norris & Ryan (1991) found that the distribution of kinematics as a function of abundance in the Carney et al. (1990) data are more consistent with a two-component model.

SDSS, with its large area coverage and accurate photometry (approaching 3% for the magnitude range of interest), is producing the best sample so far available for exploring thick-disk structure and evolution. In Figure 6, we show the CMDs (g^*, g^*-r^*) from SGS and NGS. One sees a gross bimodal structure in g^*-r^*, reflecting the separation of the halo/thick-disk ($g^*-r^* \sim 0.3$) and the thin-disk ($g^*-r^* \sim 1.3$) populations. A closer look at the blue ($g^*-r^* < 0.5$) side of Figure 6 reveals two distinct subpopulations. In the range $15 < g^* < 18$, the blue stars are dominated by the thick-disk stars, with a turnoff of $g^*-r^* \sim 0.33$. For $g^* > 18$, the Galactic halo, which has a turnoff color $g^*-r^* \sim 0.2$, becomes significant. This effect

is caused by a change from a metal-normal population to a metal-weak population. The only contaminants in our samples in this color and magnitude range are white dwarfs, QSOs, and a few RR Lyrae stars. The QSOs and white dwarfs have been removed from our samples by u^*-g^* color. Moreover, these objects are definitely rare in the thick-disk region with $g^* < 18$.

Parameters of this thick-disk population are further explored by studying a set of models.

The first is a two-component model including thin disk and halo. Such a model assumes a continuous evolutionary process throughout the lifetime of the disk after collapse. This model (hereafter Model A), based on Bahcall & Soneira (1981), is generated with only disk and halo populations, but the halo density is substantially raised (see Table 1).

The second model, a three-component model including thin disk, thick disk, and halo, assumes that a specific incident in our Galaxy's history generated an intermediate population between disk and halo. It applies two discontinuities in the dynamical, chemical, and star formation processes that govern galaxy evolution. This model, based on
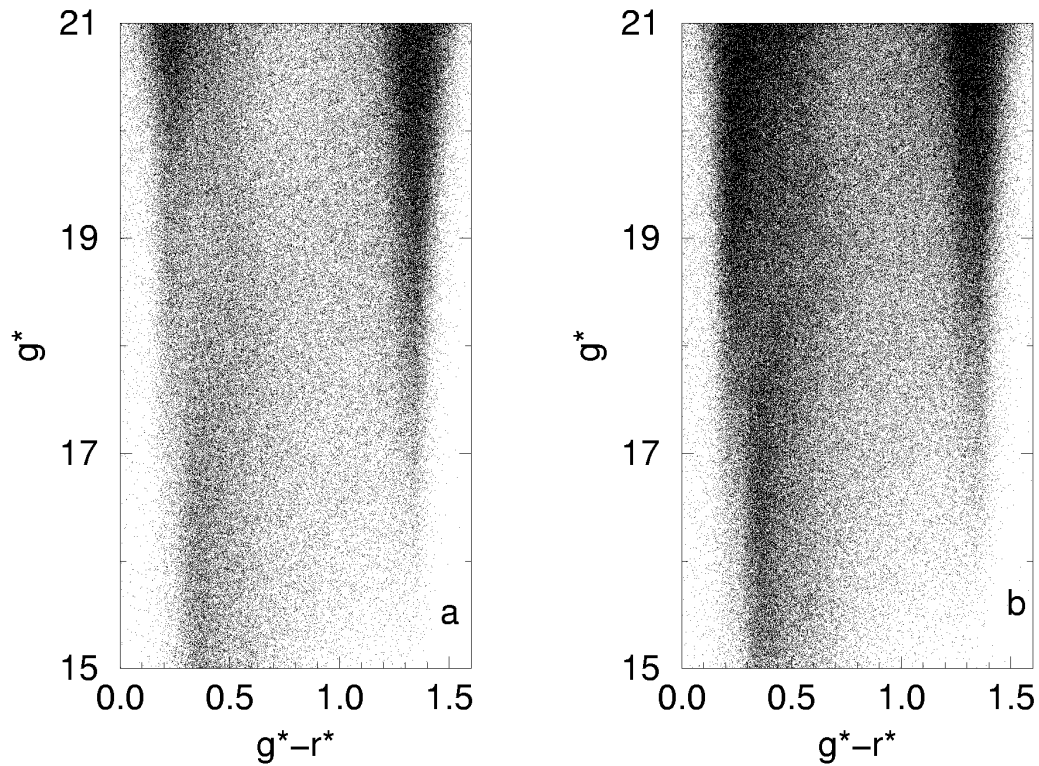
FIG. 6.—Observed (g^*, $g^* - r^*$) CMDs from (a) SGS and (b) NGS

Gilmore (1984), has a thick-disk scale height of 1300 pc with a local density of 2% of thin disk. We refer to it hereafter as Model B.

The third model (hereafter Model C) is another three-component model with enhanced thick-disk density. This model has a higher thick-disk density (13% of thin disk in the solar neighborhood) with reduced scale height (580 pc), parameters found to be consistent with the constraints of the star count data of the present study.

We have created three simulated star catalogs from the models, and we show the resulting g^*, $g^* - r^*$ CMDs for the SGS and NGS simulations for each of the three models in Figures 7 and 8, respectively. A comparison of these figures with the observed CMDs in Figure 6 shows that model A, without a thick-disk population, does not represent the observations.

Models B and C include thick-disk populations with scale heights of 1300 and 580 pc, respectively. We find that the simulated CMDs from Model C are in good agreement with the observed diagrams. Model B has a larger scale height (1300 pc), thus requiring that these stars be fainter and more distant. The thick-disk turnoff stars
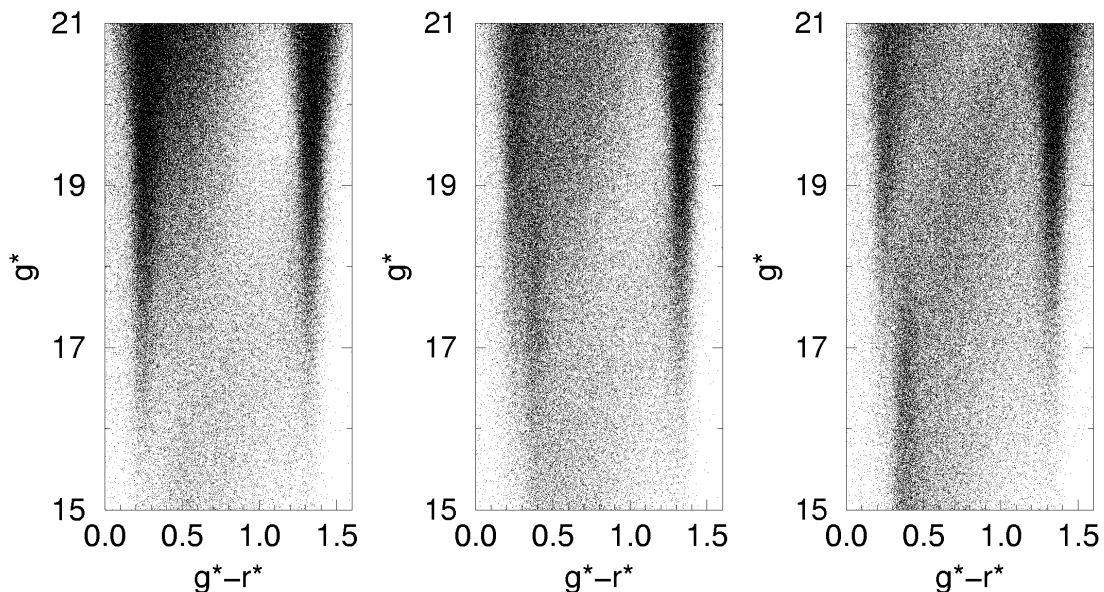

FIG. 7.—Simulated (g^*, $g^* - r^*$) CMDs from SGS. Model A (left) has no thick disk. Models B (center) and C (right) include a thick-disk population with thick-disk scale heights of 1300 and 580 pc, respectively.
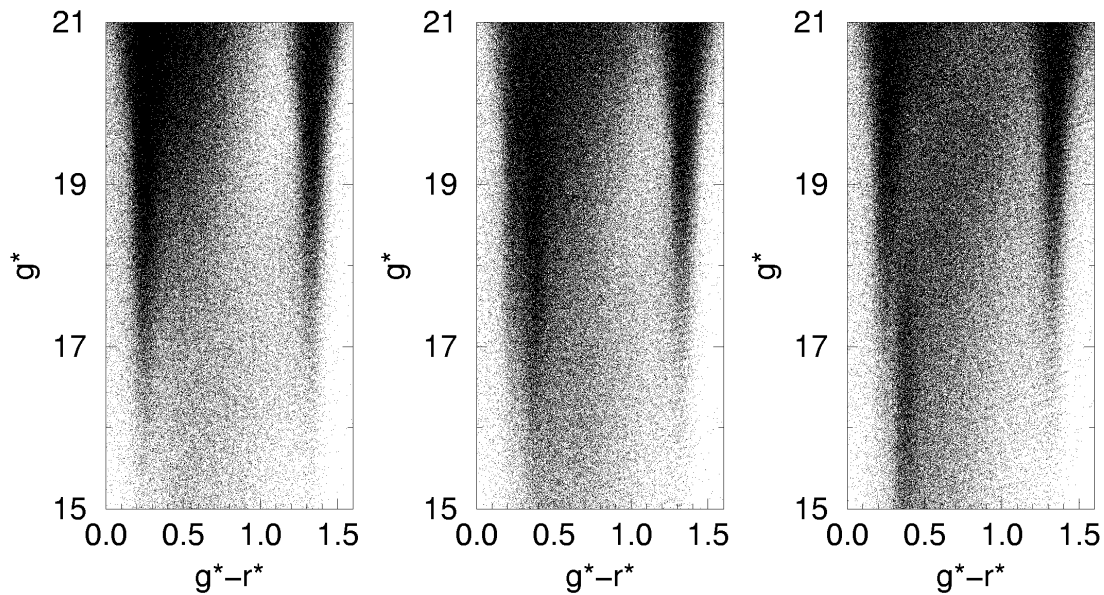
Fig. 8.—Same as Fig. 7, but for NGS

($g^*-r^* \sim 0.35$) must move toward fainter magnitudes with the larger scale height. However, from the observed CMD (Fig. 6), the thick-disk turnoff stars are invisible at $g^* < 18$ mag, indicating that Model B cannot represent the observed CMD. In the following section, we will estimate the thick-disk parameters quantitatively.

6. THE VERTICAL DISTRIBUTION OF THICK DISK

We produce a grid of star catalogs with various thick-disk scale heights and local densities and determine the best-fitting model using a maximum likelihood technique. The likelihood for each model is computed as described in Bienaymé, Robin, & Créze (1987). Let q_i be the number of stars predicted by the model in bin i and let f_i be the observed number. Then the probability that f_i is observed is

$$dP_i = (q_i^{f_i}/f_i\,!)\exp(-q_i)\,. \tag{5}$$

The likelihood of a set of q_i-values, given the relevant f_i, is

$$L = \ln \Sigma dP_i = \Sigma(-q_i + f_i \ln q_i - \ln f_i\,!)\,. \tag{6}$$

Usually, we use the reduced form to search for the models that maximize L,

$$L - L_0 = \Sigma f_i \left(1 - \frac{q_i}{f_i} + \ln \frac{q_i}{f_i}\right)\,, \tag{7}$$

where L_0 is constant and $L - L_0 = 0$ for a model which would exactly predict all f_i-values.

For each observed sample, hundreds of simulated catalogs have been generated with the thick disk's scale height varying between 200 pc and 1400 pc and its local density between 1% and 20% of the thin disk. Although the blue peak for the high-latitude population consists of a mixture of thick-disk and halo stars, at magnitudes brighter than $g^* \sim 18$ mag the thick-disk stars dominate. We choose the stars in the range $15 < g^* < 18$, where all observed stars have good u^*-g^* colors. The likelihood computation is made in bins with a step of 1 mag in g and 0.2 mag in g^*-r^* and u^*-g^*.

The thick disk's scale height is anticorrelated with its local density when fitted simultaneously. High local density is obtained in combination with small scale height, while low local density is associated with large scale height (Robin et al. 1996). In Figure 9, using the maximum likelihood technique, we show contours of equal likelihood obtained for different values of scale height and local density. Though varying results on thick-disk scale height and local normalization have been reported, we found that most of the results are along the maximum likelihood locus of Figure 9. For example, Gilmore (1984) found a scale height of 1300 pc and local normalization of 2%, Kuijken & Gilmore (1989) derived a scale height of 1000 pc and local normalization of 4%, Buser et al. (1999) have a scale height of 910 ± 300 pc with normalization $5.9\% \pm 3\%$, and Ojha et al. (1996) showed that the scale height and the local normalization are 790 pc and 6.1%. Table 4 gives the positions and values of the local maximum likelihood from contours in Figure 9 for NGS and SGS. From Figure 9 and Table 4, although it is obvious that models with a thick-disk scale height

TABLE 4
RESULTS OF LOCAL MAXIMUM LIKELIHOOD TECHNIQUE

SCALE HEIGHT (pc)	NGS		SGS	
	Local Density (%)	LML Value	Local Density (%)	LML Value
450	13	-7752	19	-5895
500	19	-5692	18	-4928
550	14.5	-5040	14.5	-4587
600	12	-4890	12	-4543
650	10.5	-4884	10	-4567
700	8.0	-4868	7.5	-4598
750	7.5	-4911	6.5	-4565
800	5.5	-5085	6.0	-4735
850	4.0	-5393	5.0	-4770
900	4.5	-5383	4	-4892
1000	3	-5942	3	-5015
1100	3	-6433	3	-5219
1200	2.0	-7009	2.5	-5498
1300	1.5	-7188	2	-5594

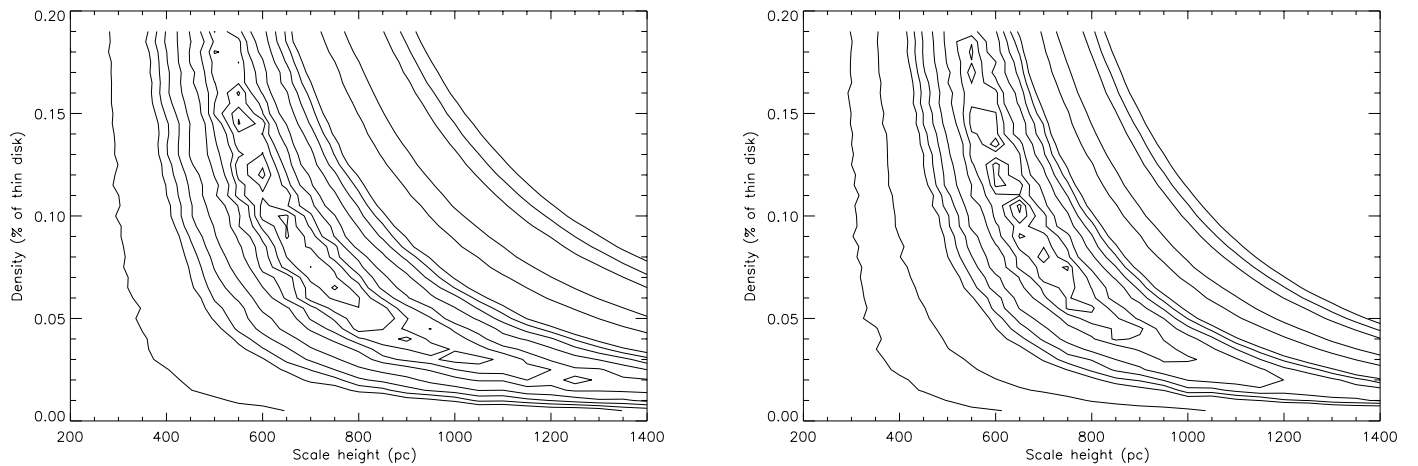NOTE.—Values of scale height correspond to contours in Fig. 9.

FIG. 9.—Contours of equal likelihood obtained for different values of thick-disk scale height and local density for SGS (*left*) and NGS (*right*)

larger than 800 pc or smaller than 550 pc cannot well represent the observations, the maximum likelihood value does not converge at a given point. In fact, the local maximum likelihood (LML) is nearly constant in a range of thick-disk scale height from 560 to 750 pc for NGS and from 600 to 750 pc for SGS. New data in other Galactic directions are needed to constrain the thick-disk parameters more accurately. From both samples, we thus quote the Galactic thick disk to have an exponential scale height of 580–750 pc and associated local density of 13%–6.5% of the local thin-disk density.

Méndez & Guzmán (1998) have analyzed pointlike sources in the Hubble Deep Field and Keck imaging, and they found an equally good match between model and observations for a thick disk with a scale height of 1300 pc (Reid & Majewski 1993) or 750 pc (Ojha et al. 1999). Robin, Reylé, & Crézé (2000) pointed out that star counts, when restricted to a small area coverage, do not give a strong constraint on the scale height. Recently, by analyzing star counts in a number of Galactic directions, Robin et al. (1996) derived a scale height of 760 pc with a local density of 5.6% of the thin disk, and Ojha et al. (1999) found a scale height of 790 pc with a local density of 6.1% of the thin disk from a photometry and proper-motion survey in two directions at intermediate latitude. These results are at the upper limit of our best maximum likelihood fit thick-disk parameters. Our results favor the small thick-disk scale height found by Robin et al. (1996) and Ojha et al. (1999), well below the original proposal of the Gilmore & Reid (1983).

7. THE DENSITY LAW OF THE HALO

Bahcall & Soneira (1981) found that the density of spheroid stars can be modeled by a deprojected de Vaucouleurs $r^{1/4}$ law with axial ratio of 0.8. Several current studies from well-identified halo tracers (Gould, Flynn, & Bahcall 1998; Sluis & Arnold 1998; Yanny et al. 2000; Ivezić et al. 2000) showed that the distribution of halo stars is well fitted by a power-law density $\rho \sim r^{-n}$. We have tested several different density laws for the halo component of the Galaxy.

Star counts that cover a significant range in Galactic coordinates, such as the present study, provide geometrical information that can be used to break degeneracies among structural parameters. In Figure 6, we can see that halo turnoff is at $g^* - r^* = 0.2$, significantly bluer than the turnoff color of the thick disk ($g^* - r^* = 0.33$). Therefore,

these stars are relatively easy to identify with accurate photometry. We selected stars with $g^* - r^*$ colors of 0.1–0.25 and $g^* > 18$ as halo turnoff star candidates. In Figure 10, we show the star counts for these stars as a function of right ascension in SGS and NGS in six g^* magnitude ranges. For SGS, we find that there are extra stars in the range $20° <$ R.A. $< 45°$ in $20.5 < g^* < 21$, and for NGS there are excess stars in the range $195° <$ R.A. $< 230°$ in $19 < g^* < 21.5$. Yanny et al. (2000) used the same samples and found large overdensities of A-colored stars at (l, b, R) of $(350°, 50°, 46$ kpc$)$ in the North and in the South at $(157°, -58°, 33$ kpc$)$, extending over tens of degrees. Using this finding from Yanny et al. (2000), we limit our samples with $g^* < 20$, where the halo streams are less important.

Figure 11 shows these star counts as a function of R.A. in SGS and NGS in the range $18 < g^* < 20$. The observed counts are shown with asterisks, and the circles and plus signs are from a power law with $(n, c/a) = (3.2, 0.8)$ and $(2.5, 0.55)$, respectively. The results from the deprojected de Vaucouleurs $r^{1/4}$ with axial ratio of 0.8 are shown by squares. We find that neither a power law with a large axial ratio (0.8) nor a de Vaucouleurs $r^{1/4}$ law with axial ratio of 0.8 fits the observed star counts as a function of right ascension. A flatter halo $(c/a = 0.55)$ with a power-law index of 2.5 is required to fit the observations. A de Vaucouleurs $r^{1/4}$ law with axial ratio of ~ 0.55 is not excluded, although a small change in another parameter for the Galactic halo (local normalization or effective radius) is necessary. This is consistent with the work of Larsen & Humphreys (1994).

In order to determine the best-fitting model using the maximum likelihood technique (eq. [7]), we produce a grid of star catalogs with varying axial ratio and power-law index. For each observed sample, 280 simulated catalogs have been generated, with axial ratio varying from 0.35 to 1.0 and the power-law index between 0.2 and 4.0. The likelihood computation is made in 20 bins with a step of $2°.52$ in R.A. for SGS and $3°$ for NGS. Figure 12 shows contours of equal likelihood obtained for different values of axial ratio and power-law index. The positions with the maximum likelihood are labeled as asterisks. We found that the best-fitting model from both samples is a flattened halo with $c/a \sim 0.55$ and a power-law index of 2.5.

To estimate the observed errors on these parameters, we divide SGS and NGS into 10 subsamples each. For each subsample, we derive the best-fitting model parameters. In
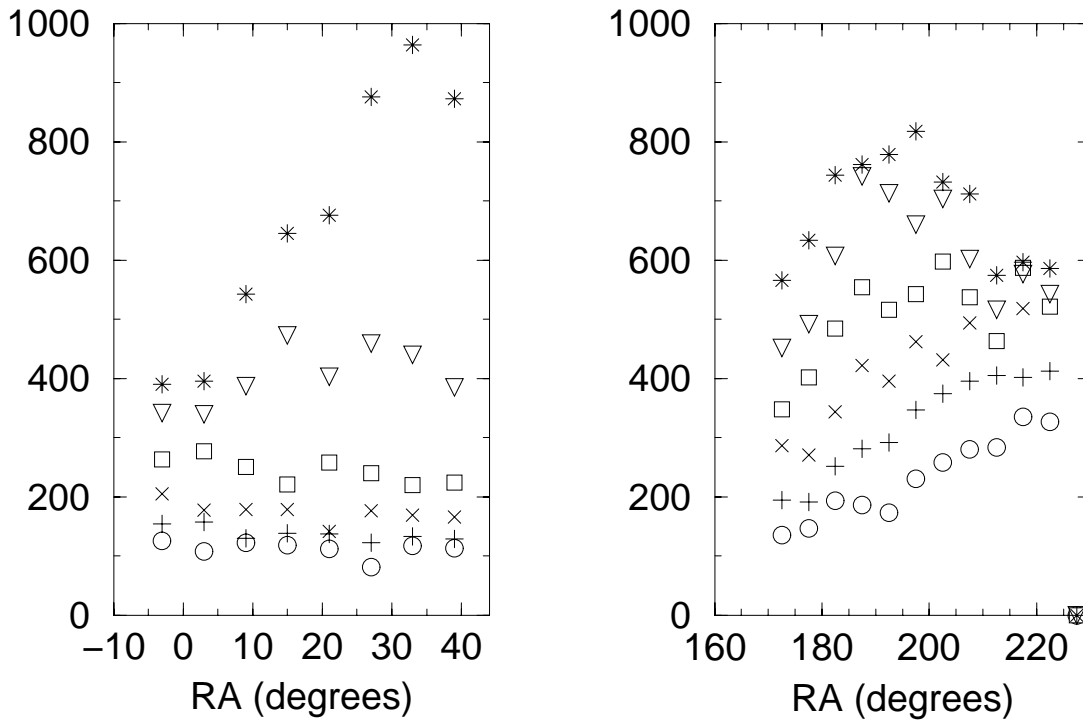
Fig. 10.—Star counts as a function of right ascension (R.A.) in SGS (*left*) and NGS (*right*) for six magnitude ranges. *Circles*: $18 < g^* \leq 18.5$; *plus signs*: $18.5 < g^* \leq 19.0$; *crosses*: $19.0 < g \leq 19.5$; *diamonds*: $19.5 < g^* \leq 20.0$; *triangles*: $20.0 < g^* \leq 20.5$; *asterisks*: $20.5 < g^* \leq 21.0$.

this way, we find the observed errors to be 0.06 and 0.3 for axis ratio and power-law index, respectively.

In order to check the influence of the choice of the halo luminosity function on these results, two different local normalizations ($0.75\rho_0$ and $1.25\rho_0$) have been adopted in our

Galaxy model. Figure 13 shows contours of equal likelihood obtained for different values of axial ratio and power-law index. The positions with the maximum likelihood are labeled as asterisks. Comparing the results of different local normalizations, we find that the choice of the local normal-
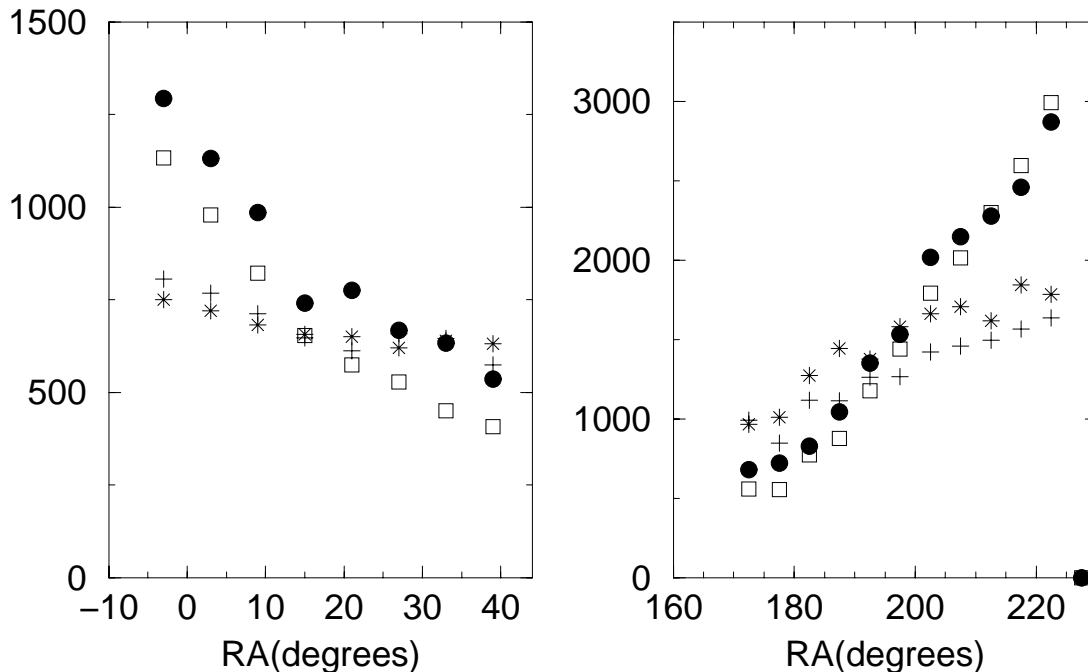

Fig. 11.—Star counts as a function of right ascension (R.A.) in SGS (*left*) and NGS (*right*) in the range $18 < g^* \leq 20$. The observed counts are shown by asterisks, and the circles and plus signs are the results from a power law with $(n, c/a) = (3.2, 0.8)$ and $(2.5, 0.55)$, respectively. The results from the deprojected de Vaucouleurs $r^{1/4}$ de Vaucouleurs (1977) law with axial ratio of 0.8 are shown by squares.
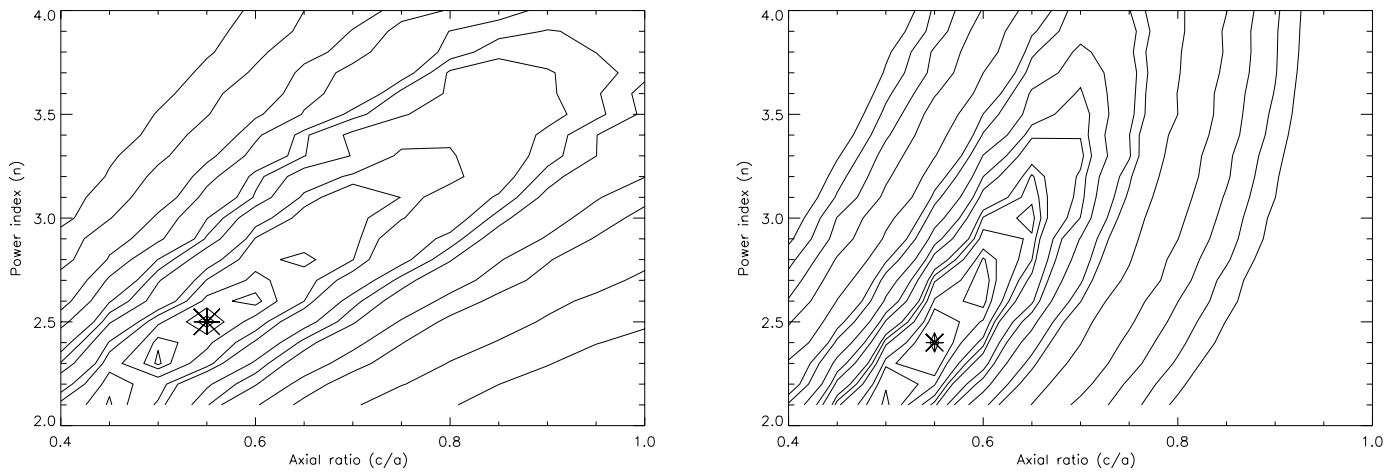
FIG. 12.—Contours of equal likelihood obtained for different values of axial ratio and power-law index for SGS (*left*) and NGS (*right*). The positions with the maximum likelihood are labeled as asterisks.

ization can displace the best-fitting model parameters slightly, but the best-fit axial ratio and power-law index are in agreement, within 1 σ, with the values derived from the standard local density (ρ_0), i.e., $c/a = 0.55$ and $n = 2.5$.

The halo density distribution has been mapped using globular clusters, RR Lyrae stars, the blue horizontal-branch (BHB) stars, and star counts. Broadly speaking, most of the early investigations showed rather steep density
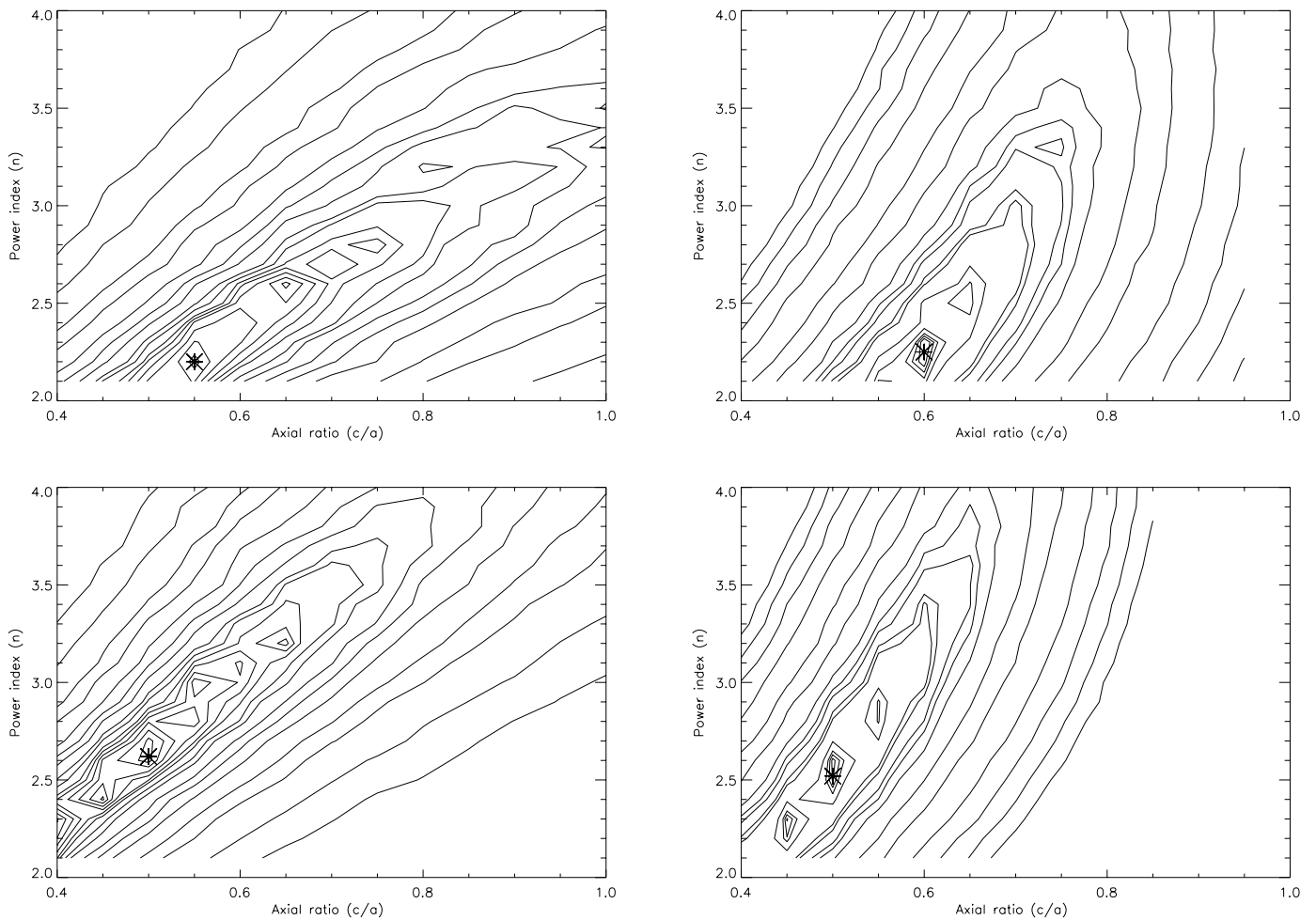

FIG. 13.—Contours of equal likelihood obtained for different values of axial ratio and power-law index. Positions with the maximum likelihood are labeled as asterisks. *Top left*: SGS with halo density $= 0.75\rho_0$, where ρ_0 is the standard local density; *bottom left*: SGS with halo density $= 1.25\rho_0$; *top right*: NGS with a halo density $= 0.75\rho_0$; *bottom right*: for NGS with halo density $= 1.25\rho_0$.

slopes, with power-law indexes of ~ 3.2 and axial ratios of ~ 0.8-0.9. Harris (1976) and Zinn (1985) have shown that the metal-weak globulars have a distribution consistent with an $r^{-3.5}$ power-law distribution. The RR Lyrae observations of Hawkins (1984) showed $n = 3.1$, with a flattening of 0.9. Bahcall & Soneira (1984) and Gilmore (1984) found axial ratios of ~ 0.8. Wyse & Gilmore (1988) reviewed different arguments based on analysis of halo-star counts and suggested a value of $c/a = 0.6$ as the optimal one. Preston et al. (1991) found that c/a increases from 0.5 to 1 up to 20 kpc with $n = 3.5$. Recently, Yanny et al. (2000) used BHB tracers from SDSS data and found $c/a = 0.65$ and $n = 3.2$. Ivezić et al. (2000) found that the RR Lyrae column density follows a shallower power law with a power-law index of 2.7. Robin et al. (2000) showed that the halo has a flattening of 0.76, and a power-law index of 2.44. We will recheck these results with forthcoming SDSS data, including RR Lyrae stars, BHB stars, and star counts in other Galactic directions in the future.

Global flattening of the Galactic dark halo has been recently investigated in detail by a number of authors (Binney et al. 1997; Sackett & Gould 1993; Nakamura, Kan-Ya, & Nishi 1996). Review of relevant literature reveals a multitude of arguments for flattened dark halos in the Milky Way and other spiral galaxies. By analyzing plots of the microlensing optical depth as a function of Galactic coordinates for different values of axis ratio c/a of the Galactic MACHO halo, Samurović, Ćirković, & Milošević-Zdjelar (1999) have shown that observations are best described by a flattened halo with $c/a \sim 0.6$. Sackett et al. (1994) use kinematics and photometry of the polar ring galaxy NGC 4650A to infer the presence of a dark matter halo and to measure its shape; they found that the dark matter halo has a vertical-to-radial axial ratio $0.3 \leq c/a \leq 0.4$. The axis ratio of the visible halo found in this paper is compatible with that of dark halo, suggesting that they have same shape and dynamical origin (Robin et al. 2000).

8. CONCLUSIONS

SDSS star counts and colors are revolutionizing our understanding of Galactic structure and evolution. The SDSS is constructing a large database that can be used for the statistical determination of the large-scale structure of the Galaxy. We have analyzed the SDSS star counts in 279 deg^2 with the help of our Galaxy model in order to parameterize the vertical distribution of stars in the Milky Way. The main results of this paper can be summarized as follows.

1. We have built a Galaxy model in the SDSS $u^*g^*r^*i^*z^*$ photometric system. Observations (Smith et al. 2001) for the calibration and definition of the standard stars are used to obtain transformation equations from the Johnson UBV system to SDSS $u^*g^*r^*i^*z^*$ system. While this model needs to be refined in many respect in the future, it can provide a suitable framework for interpreting SDSS data in its present form.

2. Using two large star count samples (NGS and SGS), we have determined that the Sun's distance is 27 ± 3 pc above the Galactic midplane and that the scale height of the thin disk is 330 ± 4 pc.

3. A distinct thick-disk population can be clearly identified from the CMD. Its turnoff is ~ 0.1 mag redder in $g^* - r^*$ than that of the halo population, and it clearly has

large numbers of blue stars fainter than those predicted by a thin-disk population.

4. The vertical distribution of the thick disk has been determined using a maximum likelihood technique. Our best-fit model gives a thick-disk scale height between 580 and 750 pc, with a local density of 13–6.5% of the thin disk.

5. The density law for the halo population of the Galaxy is investigated. We find that the data support a flattened halo with $c/a \sim 0.55 \pm 0.06$ and a power-law index of 2.5 ± 0.3. The axis ratio of the visible halo found in this paper is compatible with that of the dark halo (Sackett et al. 1994; Samurović et al. 1999), suggesting that they have same shape and dynamical origin.

Thick-disk formation scenarios are generally explained by "top-down" and "bottom-up" models (Majewski 1993 and references therein). For the top-down scenarios (the pre-thin models), the thick disk arises during a transitional phase between the formation of the halo and the thin disk, it is considered to be a dissipative, rotationally-supported structure, and the thin disk represents the final stage in the dissipative settling of disk gas. The chemical and kinematic properties of the thick disk and thin disk are rather smoothly joined (Sandage 1990; Larson 1976; Gilmore 1984; Wyse & Gilmore 1988; Burkert, Truran, & Hensler 1992).

Of the many bottom-up scenarios (post-thin models) that have been proposed for the origin of the thick disk, Norris (1987) suggested that the secular kinematic diffusion of thin-disk stars, such as disk-star scattering on giant molecular clouds (Spitzer & Schwarzschild 1951, 1953), and/or scattering by spiral features (Barbanis & Woltjer 1967; Jenkins & Binney 1990) may produce the Galactic thick disk. Quinn, Hernquist, & Fullagar (1993) proposed a thick-disk model based on a scenario of satellite accretion by a spiral galaxy. In their N-body simulation, Quinn et al. (1993) follow the evolution of a satellite galaxy, initially in a prograde, circular orbit about a disk of mass 10 times that of the satellite, with the orbit inclined 30° to the plane of the disk, at a Galactocentric radial distance of 6 disk scale lengths. Their model leaves several important observational signatures. First, the thick disk is a separate population distinct from the thin disk and the halo. Second, the vertical heating increases the disk scale height by a factor of 2. All our results are compatible with the resulting thick-disk characteristics from the disruptive heating of a preexisting thin disk by satellite galaxy accretion (Quinn et al. 1993). The stars of such accreted satellites may still be identifiable from all-sky surveys with good photometry in several bands and robust star-galaxy separation. Using SDSS data, Yanny et al. (2000) found that the Milky Way contains huge clumps of stars that appear to be the remains of smaller galaxies. Ivezić et al. (2000) searched SDSS data for RR Lyrae stars and found that the Galactic distribution of stars in their sample shows a clump, supporting the merger/accretion scenario.

REFERENCES

Adelman, J., et al. 1999, AAS, 195, 82.04
Bahcall, J. N. 1986, ARA&A, 24, 577
Bahcall, J. N., Ratnatunga, K. U., Buser, R., Fenkart, R. P., & Spaenhauer, A. 1985, ApJ, 299, 616
Bahcall, J. N., & Soneira, R. M. 1981, ApJS, 47, 357
———. 1984, ApJS, 55, 67
Barbanis, B., & Woltjer, L. 1967, ApJ, 150, 461
Bienaymé, O., Robin, A. C., & Crézé, M. 1987, A&A, 180, 94
Binney, J., Gerhard, O., & Spergel, D. 1997, MNRAS, 288, 365
Burkert, A., Truran, J. W., & Hensler, G. 1992, ApJ, 391, 651
Buser, R., Rong, J., & Karaali, S. 1999, A&A, 348, 98
Carney, B. W., Aguilar, L., Latham, D. W., & Laird, J. B. 1990, AJ, 99, 201
Chen, B. 1997, ApJ, 491, 181
Chen, B., Figueras, F., Torra, J., Jordi, C., Luri, X., & Galadí-Enríquez, D. 1999, A&A, 352, 459
Cohen, M. 1995, ApJ, 444, 874
Conti, P. S., & Vacca, W. D. 1990, AJ, 100, 431
de Vaucouleurs, G. 1977, AJ, 82, 456
Einasto, J. 1979, in IAU Symp. 84, Large Scale Characteristics of the Galaxy, ed. W. B. Burton (Dordrecht: Reidel), 451
Fan, X. 1999, AJ, 117, 2528
Fukugita, M., Ichikawa, T., Gunn, J. E., Doi, M., Shimasaku, K., & Schneider, D. P. 1996, AJ, 111, 1748
Gilmore, G. 1984, MNRAS, 207, 223
Gilmore, G., & Reid, N. 1983, MNRAS, 202, 1025
Gould, A., Flynn, C., & Bahcall, J. N. 1998, ApJ, 503, 798
Gunn, J. E., et al. 1998, AJ, 116, 3040
Hammersley, P. L., Garzón, F., Mahoney, T., & Calbet, X. 1995, MNRAS, 273, 206
Harris, W. E. 1976, AJ, 81, 1095
Hawkins, M. R. S. 1984, MNRAS, 206, 433
Haywood, M., Robin, A. C., & Crézé, M. 1997, A&A, 320, 428
Humphreys, R. M., & Larsen, J. A. 1995, AJ, 110, 2183
Ivezić, Ž., et al. 2000, AJ, 120, 963
Jenkins, A., & Binney, J. 1990, MNRAS, 245, 305
Johnson, H. L. 1965, ApJ, 141, 170
———. 1966, ARA&A, 4, 193
Keenan, P. C. 1963, in Basic Astronomical Data, ed. K. A. Strand (Chicago: Univ. Chicago), 78
Kron, R. G. 1978, Ph.D. thesis, Univ. California, Berkeley
Kuijken, K., & Gilmore, G. 1989, MNRAS, 239, 605
Larsen, J. A., & Humphreys, R. M. 1994, ApJ, 436, L149
Larson, R. B. 1976, MNRAS, 176, 31
Lupton, R. H., et al. 2001, in preparation
Majewski, S. R., 1991, Ph.D. thesis, Univ. Chicago
———. 1993, ARA&A, 31, 575
McCuskey, S. W. 1966, Vistas Astron., 7, 141
Méndez, R. A., & Guzmán, R. 1998, A&A, 333, 106

Méndez, R. A., & van Altena, W. F. 1998, A&A, 330, 910
Morgan, J. G., & Eggleton, P. P. 1978, MNRAS, 182, 219
Nakamura, T., Kan-Ya, Y., & Nishi, R. 1996, ApJ, 473, L99
Norris, J. 1987, AJ, 93, 616
Norris, J. E., & Ryan, S. G. 1991, ApJ, 380, 403
Ojha, D. K., Bienaymé, O., Mohan, V., & Robin, A. C. 1999, A&A, 351, 945
Ojha, D. K., Bienaymé, O., Robin, A. C., Crézé, M., & Mohan, V. 1996, A&A, 311, 456
Pandey, A. K., Bhatt, B. C., Mahra, H. S. 1988, A&A, 189, 66
Peterson, B. A., Ellis, R. S., Kibblewhite, E. J., Bridgeland, M. T., Hooley, T., & Horne, D. 1979, ApJ, 233, L109
Phleps, S., Meisenheimer, K., Fuchs, B., & Wolf, C. 2000, A&A, 356, 108
Pier, J. R., et al. 2001, in preparation
Preston, G. W., Shectman, S. A., & Beers, T. C. 1991, ApJS, 76, 1001
Quinn, P. J., Hernquist, L., & Fullagar, D. P. 1993, ApJ, 403, 74
Ratnatunga, K. U., & Yoss, K. M. 1991, ApJ, 377, 442
Reid, I. N., & Majewski, S. R. 1993, ApJ, 409, 635
Robin, A. C., & Crézé, M. 1986, A&A, 157, 71
Robin, A. C., Haywood, M., Crézé, M., Ojha, D. K., & Bienaymé, O. 1996, A&A, 305, 125
Robin, A. C., Reylé, C., & Crézé, M., 2000, A&A, 359, 103
Sackett, P. D., & Gould, A. 1993, ApJ, 419, 648
Sackett, P. D., Rix, H.-W., Jarvis, B. J., & Freeman, K. C. 1994, ApJ, 436, 629
Samurović, S., Ćirković, M. M., & Milošević-Zdjelar, V. 1999, MNRAS, 309, 63
Sandage, A. 1970, ApJ, 162, 841
———. 1990, JRASC, 84, 70
Schmidt, M. 1975, ApJ, 202, 22
Sluis, A. P. N., & Arnold, R. A. 1998, MNRAS, 297, 732
Smith, A., et al. 2001, in preparation
Spagna, A., Lattanzi, M. G., Lasker, B. M., McLean, B. J., Massone, G., & Lanteri, L. 1996, A&A, 311, 758
Spitzer, L., Jr., & Schwarzschild, M. 1951, ApJ, 114, 385
———. 1953, ApJ, 118, 106
Stobie, R. S., & Ishida, K. 1987, AJ, 93, 624
Stothers, R., & Frogel, J. A., 1974, AJ, 79, 456
Tyson, J. A., & Jarvis, J. F. 1979, ApJ, 230, L153
Wielen, R., Jahreiss, H., & Kruger, R. 1983, in IAU. Colloq. 76, Nearby Stars and the Stellar Luminosity Function, ed. A. G. Davis Phillip & A. R. Upgren (Schenectady: L. Davis), 163
Wyse, R. F. G., & Gilmore, G. 1988, AJ, 95, 1404
Yamagata, T., & Yoshii, Y. 1992, AJ, 103, 117
Yanny, B., et al. 2000, ApJ, 540, 825
York, D. G., et al. 2000, AJ, 120, 1579
Yoshii, Y., Ishida, K., & Stobie, R. S. 1987, AJ, 92, 323
Zinn, R. 1985, ApJ, 293, 424